

A Dual-Band, Dual-Pattern Antenna for Body-Centric Communications

Mohammed A. Alqarni

College of Computer Science and Engineering, Department of Software Engineering, University of Jeddah, Jeddah, Saudi Arabia
alqarni@uj.edu.sa

Rizwan Masood

Deanship of Research and Development Project, University of Jeddah, Jeddah, Saudi Arabia
rmasood@ieee.org

Mohammed Saeed Alkatheri

College of Computer Science and Engineering, Department of Cybersecurity, University of Jeddah, Jeddah, Saudi Arabia
msalkatheri@uj.edu.sa

Sajjad Hussain Chauhdary

College of Computer Science and Engineering, Department of Computer Science and Artificial Intelligence, University of Jeddah, Jeddah, Saudi Arabia
shussain@uj.edu.sa (corresponding author)

Sajid Saleem

College of Computer Science and Engineering, Department of Computer and Network Engineering, University of Jeddah, Jeddah, Saudi Arabia
sssaleem@uj.edu.sa

Received: 6 June 2024 | Revised: 15 July 2024 | Accepted: 26 July 2024

Licensed under a CC-BY 4.0 license | Copyright (c) by the authors | DOI: <https://doi.org/10.48084/etasr.8051>

ABSTRACT

A dual-band, dual-pattern antenna is presented for 1.437 GHz L-band and 2.45 GHz Industrial Scientific and Medical (ISM) band applications. The antenna is based on multilayer circular patches with symmetric slots and two asymmetric cylindrical vias that shorten the multiple layers with the ground plane using Plated Through-Holes (PTHs) to generate the required resonant modes. The first mode is operated at 1.437 GHz, providing an omnidirectional radiation pattern, while the second mode is operated at 2.45 GHz, providing a directional or broadside radiation pattern. The antenna was fabricated to validate the simulation results and excellent agreement was found between the simulation and experimental results. The antenna has a total size of only $6 \times 6 \times 0.443 \text{ cm}^3$, which corresponds to an electrical size of $0.5\lambda_0 \times 0.5\lambda_0 \times 0.03\lambda_0$ at 2.45 GHz and $0.28\lambda_0 \times 0.28\lambda_0 \times 0.02\lambda_0$ at 1.437GHz, thanks to the loading effect of shorting vias. The gain of the antenna is 1.62 dBi at 1.437 GHz and 6.48 dBi at 2.45 GHz, along with quite good radiation efficiencies of 83.4% and 96%, respectively. For body-centric applications, the performance of the antenna was also examined in close proximity to the human body. Nearly stable performance was found in close proximity to the human body, comparable to free space performance in terms of both impedance matching and radiation patterns. The 10g Specific Absorption Rate (SAR) of the antenna was also measured and found to be below the international compliance limits. These characteristics make the antenna a very promising choice for body-centric communications. The antenna also applies to other wireless systems such as MIMO, wireless ad hoc networks, etc. It offers radiation pattern diversity in a single planar package with a highly flexible and adaptable design by providing much more degrees of freedom than classical microstrip antennas.

Keywords-body-centric communication; dual pattern antenna; MIMO; radiation pattern diversity; SAR

I. INTRODUCTION

Wireless Body Area Sensor Networks (WBASNs) are short-range Wireless Sensor Networks (WSNs) that operate in close proximity to the human body, providing a network of wireless sensors or devices. They can collect and interpret human vital signs or other physiological data and find potential use in a wide range of applications, such as smart home, healthcare services, disability assistance, surveillance, sports, security, etc. The wireless sensors of a WBASN can collect human physiological data and communicate them to a central processing node (Body Area Coordinator/Aggregator), which serves as a central node to perform functions, including sensing, data fusion, processing, etc. The Body Area Coordinator/Aggregator also serves as a gateway between WBASNs and between the WBASN and the next higher-level infrastructures such as hospitals and retirement communities [1]. For body-centric communication, devices can communicate at two hierarchical levels for wireless transmission, namely on-body and off-body, as shown in Figure 1. On-body communication involves communication between two sensors located on different parts of a human subject, whereas off-body communication occurs when a body-worn sensor (e.g., BAN aggregator) communicates with an external access point such as a gateway or Base Station (BS) for wireless transmission of physiological or recorded data.

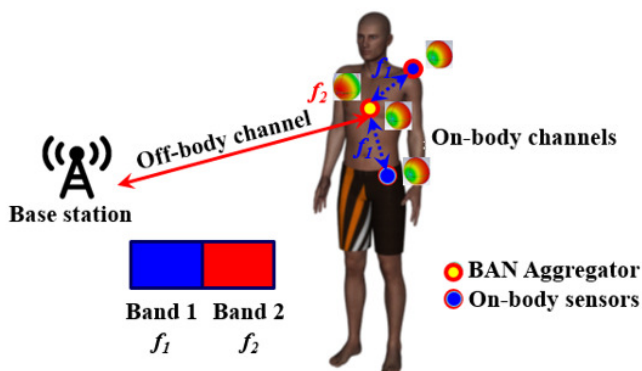


Fig. 1. On- and off-body communication channels along with optimal antenna radiation patterns in a WBASN perspective.

From an antenna perspective, two different types of radiation patterns are required for wearable applications, as evidenced in Figure 1. For on-body communication, an omnidirectional radiation pattern is required, which is known to induce surface or creeping waves that can enhance on-body propagation [2]. For off-body communication, the antenna should radiate away from the body or in the broadside direction to improve the link budget, since the gateway or BS is located away from the body. This means that antennas with different forms of radiation patterns are required depending on the on-body or off-body communication requirements, as observed in Figure 1. The simplest way to achieve radiation pattern diversity is to use two different antennas optimized for the required frequency bands and arranged in space diversity, but this demands at least a quarter-wavelength or preferably a half-wavelength separation at the operating frequency. This is not

an optimal solution for WBASNs, which have stringent footprint and form factor requirements as the sensors operate in close proximity to the human body. The optimal situation is to use a pattern diversity antenna in a single planar package, which can provide the required radiation patterns for both on- and off-body communications at different frequency bands. This also helps to reduce the interference problem, as the different sensors can then communicate simultaneously in full-duplex mode with other on- or off-body nodes.

A number of antennas have been presented in the literature for WBAN applications, such as Planar Inverted-F Antenna (PIFA) [3], antennas based on Electromagnetic Bandgap (EBG) [4], or Artificial Magnetic Conductor (AMC) [5-7]. In addition, antennas based on Coplanar Waveguide (CPW) [8] or microstrip ring resonator [9] have also been proposed for body-centric communication. Most of these antennas operate in single mode. In addition, antennas have been designed to operate primarily in on-body mode [10-12] or off-body mode [13]. However, to meet both on and off-body communication needs, the antenna must operate in dual modes with dual radiation characteristics. A dual-band wearable button antenna was proposed in [14] for WBAN applications, which provides omnidirectional radiation for on-body communication (2.33-2.62 GHz) and broadside radiation for off-body communication (5.13-8.03 GHz). The antenna has a compact size, but offers relatively low efficiency (about 70% in free space). A dual-band, dual-mode patch antenna was introduced in [15] for WBAN on-on-off repeater systems. The antenna provides vertical monopole-like radiation in the 2.45 GHz ISM band and horizontal monopole-like radiation in the 5.8 GHz ISM band. A dual-band, dual-mode patch antenna was presented in [16], where TM_{11} and TM_{02} modes were excited at 2.45 GHz and 5.8 GHz for off- and on-body-centric communication, respectively. Authors in [17], proposed a dual-band, dual-mode patch antenna for on/off body communications. This antenna provides an omnidirectional radiation pattern at 2.45 GHz and a broadside radiation pattern at 5.8 GHz. However, the gain of the antenna appears to be relatively reduced at the lower ISM band (2.45 GHz) in the azimuth plane (maximum gain of -0.762 dBi), which could potentially be a significant issue for on-body links. A pattern reconfigurable antenna was proposed in [18] for use in both on- and off-body modes at the ISM 2.4-GHz band, employing the usage of p-i-n diodes. Another dual-band patch antenna with paired L-shaped slots was presented in [19] for 2.45-5.8 GHz on and off-body communications. A microstrip-fed ground-modified antenna with pattern selectivity at 2.4 GHz was introduced in [20], which can offer either omnidirectional mode or two directional modes, which can be shifted by 180° using switches. However, the antenna features a meandered ground plane and includes slots, which may impede its performance in a body-centric environment. A CPW-based patch antenna was proposed in [21] for 2.4 GHz and 5.8 GHz on-/off-body communications. The antenna exhibits a broadside radiation pattern in the 2.4 GHz ISM band and a monopole-like radiation pattern in the 5.8 GHz ISM band. Another CPW-based dual-band patch antenna was presented in [22], which offers radiation pattern diversity at two frequencies with a relatively narrow gap (5.16 GHz and 5.48 GHz). The antenna offers dual directional radiation at 5.16

GHz and directional radiation pattern at 5.48 GHz. The measured peak gain of the antenna at 5.16 GHz is 1.13 dBi, along with a radiation efficiency of 31%. At 5.48 GHz, the measured peak gain is 2.81 dBi along with a radiation efficiency of 30.4% in free space, which are relatively low values.

A wearable dual-band antenna was presented in [23] for high gain, directional radiation pattern along with low SAR for 2.45/3.45 GHz off-body communication. A compact dual-band wearable antenna was introduced in [24], for 2.4 GHz and 5.8 GHz WBAN applications on a semi-flexible Rogers Duroid RO3003 substrate. However, the antenna in question lacks a full ground plane, which can be crucial for WBAN applications. A wideband wearable metasurface antenna was proposed for dual-band WBAN operation with on- and off-body modes at 2.45 and 5 GHz, respectively [25]. A dual-band antenna designed for use on the wrist, based on Composite Right and Left-Handed Transmission Lines (CRLH-TLs), was proposed for integration into smartwatches [26]. The antenna offers polarization diversity at 2.4 and 5.8 GHz WLAN bands with compliant SAR values. A flexible dual-band wearable antenna was introduced for off and on-body communications on a hybrid dielectric substrate, namely, flexible Polydimethylsiloxane (PDMS) and PF4-foam materials. The antenna provides broadside radiation pattern at ISM 2.45 GHz and omnidirectional radiation at 5.8 GHz [27]. However, most of these antennas have complex geometries and are difficult to be modified to provide pattern diversity at exact required frequency bands.

Examining the various limitations of state-of-the-art antennas, there is a potential need for a simplistic and more adaptable dual-band antenna with a greater number of degrees of freedom. The antenna should be capable of generating a radiation pattern that allows for both on- and off-body communication in a single planar package, while maintaining stable on-body performance. This paper presents a novel dual-band, dual-pattern antenna that successfully generates the requisite radiation pattern diversity for both on- and off-body communications. Additionally, the antenna offers a highly flexible and adaptable design, allowing for precise tuning or modification to accommodate any desired frequency bands. The design is based on a stacked configuration of circular patches, incorporating both symmetrical slots and asymmetrical shorting vias within a single planar package. This approach offers a total of 14 degrees of freedom, allowing for optimization of the antenna for any required frequency bands. One of the most straightforward applications of this antenna is in a WBASN context, where it can be used to record physiological data from different on-body sensors and transmit it to a central BAN controller via the on-body mode of the antenna. Subsequently, the central node can process all received data and transmit them to a WLAN network through the off-body mode of the antenna for further processing.

II. ANTENNA DESIGN

The proposed antenna design is based on two circular patches with symmetrical slots, which are stacked on two identical substrates and two shorting vias, which serve to create the necessary resonant modes. Additionally, the shorting stubs

contribute to reducing the overall size of the antenna due to the loading effect, as previously discussed in [28]. The antenna has a full ground plane at the backside, as shown in Figure 2. The antenna was simulated in Computer Simulation Technology (CST) Microwave Studio (MWS) [29] using the time domain solver, following an exhaustive and careful parametrization campaign in which all available degrees of freedom were utilized to excite the two required resonant modes at 1.437 GHz (f_{r1}) and 2.45 GHz (f_{r2}).

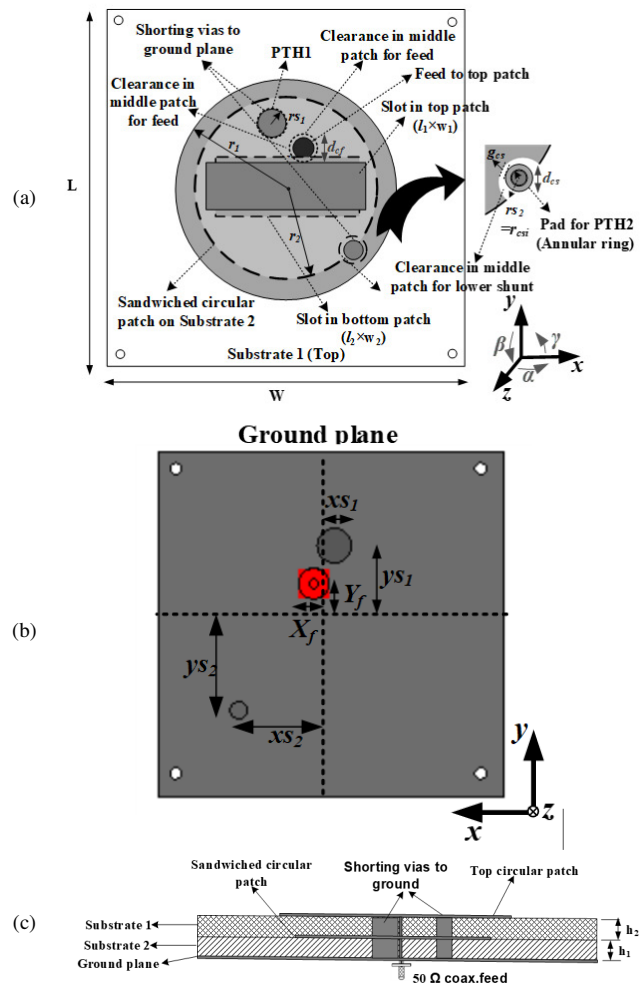


Fig. 2. Layout of the antenna (substrate RT5870, $\epsilon_r = 2.33$, $h_1 = h_2 = 2.18$ mm) (a) top view (b) back view (c) side view. The center in both (a) and (b) corresponds to the origin (0, 0).

The design is composed of two analogous substrates, namely Rogers RT5870, which exhibit a dielectric constant (ϵ_r) of 2.33, a thickness (h) of 2.18 mm, a loss tangent ($\tan\delta$) of 0.0012, and a Cu cladding of 35 microns. The left shunt (rs_1) is shorted between all three layers, namely the top patch, intermediate patch, and bottom ground plane. In contrast, the right shunt (rs_2) is only shorted between the top layer and bottom ground plane (Figure 2). To ensure robust connectivity between multiple layers and to circumvent the potential issues arising from soldering between substrates during measurement,

this study employed the use of Plating Through Hole (PTHs) across multiple layers for the two shorting vias (PTH1 and PTH2, as illustrated in Figure 2). Given that the electric field inside a metallic cylinder is zero and only propagates through the surface of the conductor, the PTHs had a negligible impact on the antenna response once the shorting cylinders were inserted in the vias. A pad was placed on the middle patch, situated across the junction of the PTH2. This was followed by trimming of the patch edge (equivalent to an antipad), with the objective of providing clearance, given that the middle patch is not shorted with the lower shunt, in order to ensure the desired operation of the antenna. The dimensions of this annular ring, portrayed in Figure 2(a), were optimized through simulation, with inner and outer radii of 1.5 mm and 2.3 mm, respectively. This configuration provides a clearance gap of 0.7 mm from the periphery of the intermediate patch, as presented in Table 1. Ultimately, the two shorting cylinders were directly inserted into the PTHs. This approach also facilitated the avoidance of soldering in the middle layer during measurement, thereby circumventing the issue of spacing introduced by soldering, which is a crucial factor affecting the overall response. The antenna is fed through a coaxial feed, which is connected to the top patch through the intermediate patch. This configuration provides clearance for the feed probe. The dimensions of this via (d_{cp}) were determined through thorough simulation to prevent any coupling caused by the feed probe with the intermediate patch. In order to ensure the highest degree of realism and accuracy in the simulation, the exact parameters were employed, as would be done in an actual measurement. For instance, the precise loss tangent of RT5870 was considered, and copper was used to model all metallic layers in place of PEC. Additionally, a physical model of a 50 Ω coaxial connector was constructed in CST MWS in lieu of a discrete port. Finally, to ensure reliable accuracy, the mesh convergence was also investigated in CST MWS using an energy-based refinement criterion (error, $\Delta < 2\%$). These considerations enabled the acquisition of the most precise measurement in accordance with the simulation results.

The current vector distribution of the antenna for the two resonant frequencies is depicted in Figure 3. The rectangular slot causes the current to flow around it (in comparison to the slotless scenario), thereby increasing the electrical length and shifting the resonance to a lower frequency. Furthermore, the current vectors are oriented in the same direction in the xy -plane at 2.45 GHz, resulting in maxima in the broadside direction. In contrast, the y -current components are also generated at 1.437 GHz in the region surrounding the shorting vias, which can be attributed to the short-circuit loading effect, as previously discussed in [28]. The vector addition of the x and y -components of the current ultimately yields an omnidirectional radiation pattern at 1.437 GHz. The three-dimensional radiation patterns of the antenna for the optimized design are presented in Figure 4 for both resonant modes. As it can be observed, the antenna exhibits omnidirectional radiation at 1.437 GHz and broadside radiation at 2.45 GHz. The maximum gain of the antenna is 1.62 dBi at 1.437 GHz and 6.48 dBi at 2.45 GHz, with corresponding radiation efficiencies of 83.4% and 96%, respectively. The second resonant mode demonstrates higher gain and efficiency compared to the first

mode, which can be attributed to the directive nature of the pattern. This is desirable for the off-body mode due to the increased distance of the gateway from the body.

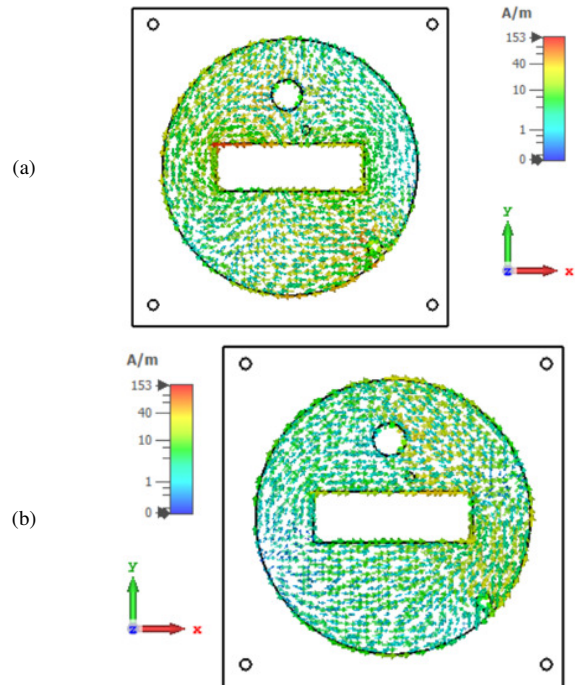


Fig. 3. Surface current distribution of the antenna at (a) 1.437 GHz and (b) 2.45 GHz on same scale.

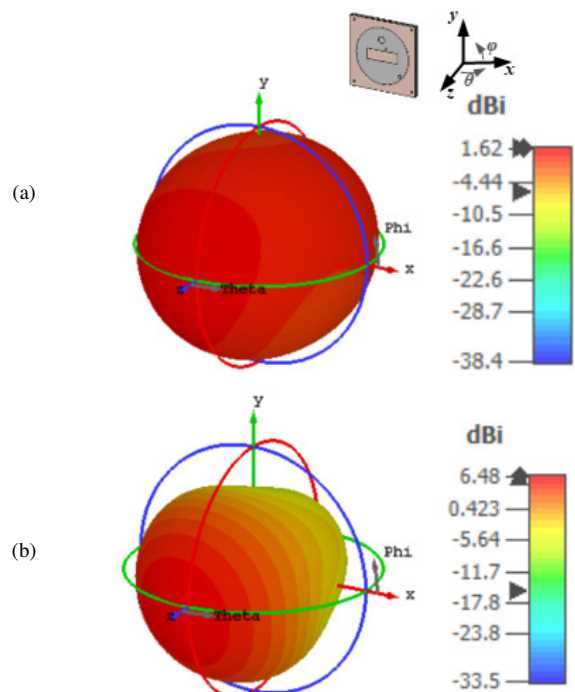


Fig. 4. 3D radiation patterns of the antenna at (a) 1.437 GHz and (b) 2.45 GHz. The coordinate system is also shown.

III. SIMULATION AND EXPERIMENTAL RESULTS

To achieve the desired resonance at the requisite frequency bands, an exhaustive and rigorous simulation was performed in CST MWS, using all fourteen available degrees of freedom for the specified substrates. These degrees of freedom include r_1 , r_2 , r_{s1} , r_{s2} , l_1 , w_1 , l_2 , w_2 , x_{s1} , y_{s1} , x_{s2} , y_{s2} , X_f and Y_f , as evidenced in Figure 2. The influence of specific dimensions on the resonant frequencies of the two modes is presented in Figure 5. The radius of the top patch, r_1 , exerts a predominant influence on both the upper and lower resonant frequencies, designated as f_{r1} and f_{r2} , respectively. As the radius r_1 is increased, both resonant frequencies f_{r1} and f_{r2} are decreasing, as a consequence of the corresponding increase in the electrical length of the antenna. An increase in the radius of either shunt (r_{s1} or r_{s2}) results in an elevation of both resonant frequencies (f_{r1} and f_{r2}). However, this is associated with a trade-off between matching or return loss at the two resonant frequencies (f_{r1} , f_{r2}) for the lower shunt (r_{s2}). Similarly, the positioning of the two shorting vias (x_{s1} , y_{s1}) and (x_{s2} , y_{s2}) influences the distance between the two resonant frequencies (f_{r1} and f_{r2}), as well as the impedance matching. As shown in Figure 5(c), the lower shunt results in the greatest reduction of the lower resonant frequency (f_{r1}) by shifting it toward the right edge of the patch, thereby reducing the overall size of the patch. The slots were removed from the circular patches with the objective of reducing the antenna size further by lowering the resonant frequency (assuming that the dimensions other than the slot length were constant) and improving impedance matching. An increase in either of the slot lengths (l_1 and l_2 in Figure 2) or an increase in the slot widths (w_1 and w_2 in Figure 2) results in a reduction in the upper resonant frequency (f_{r2}), while the lower resonant frequency (f_{r1}) remains relatively unaffected. The positioning of the feed (X_f , Y_f) primarily influences the matching or return loss of both modes. A number of trade-offs were identified between different parameters in terms of impedance matching, resonant frequencies, and the gap between them. Ultimately, an exhaustive parameterization was conducted in CST MWS, following a comprehensive investigation of the fourteen degrees of freedom and their interdependence. The aforementioned parameters were ultimately optimized with the objective of exciting the two resonant modes at 1.437 GHz L-band and 2.45 GHz ISM band. The comprehensive optimized dimensions are showcased in Table I, which was obtained following a rigorous investigation of all parameters in CST MWS, while simultaneously addressing the various trade-offs.

TABLE I. OPTIMIZED DIMENSIONS OF THE ANTENNA

L	W	r_{s1}	r_{s2}	r_1	r_2	l_1	w_1	l_2	w_2
60 mm	60 mm	3 mm	1.5 mm	24.2 mm	22.2 mm	28 mm	9 mm	26 mm	9 mm
x_{s1}	y_{s1}	x_{s2}	y_{s2}	g_{es}	d_{cf}	r_{csi}	d_{cs}	X_f	Y_f
-0.6 mm	13.6 mm	16 mm	-15 mm	0.7 mm	4 mm	1.5 mm	4.6 mm	3 mm	7 mm

To validate the simulated results, a prototype of the antenna was also fabricated using Rogers RT5870 laminate with a dielectric constant (ϵ_r) of 2.33 and a thickness (h) of 2.18 mm, which were also utilized in the simulation. Fabrication was performed deploying Leiterplatten-Kopierfräsen (LPKF) laser prototyping. The antenna was powered by a 50 Ω coaxial line

feed, which stimulated the top patch through a clearance hole in the intermediate patch ($d_{cf} = 4$ mm), as done in the simulation.

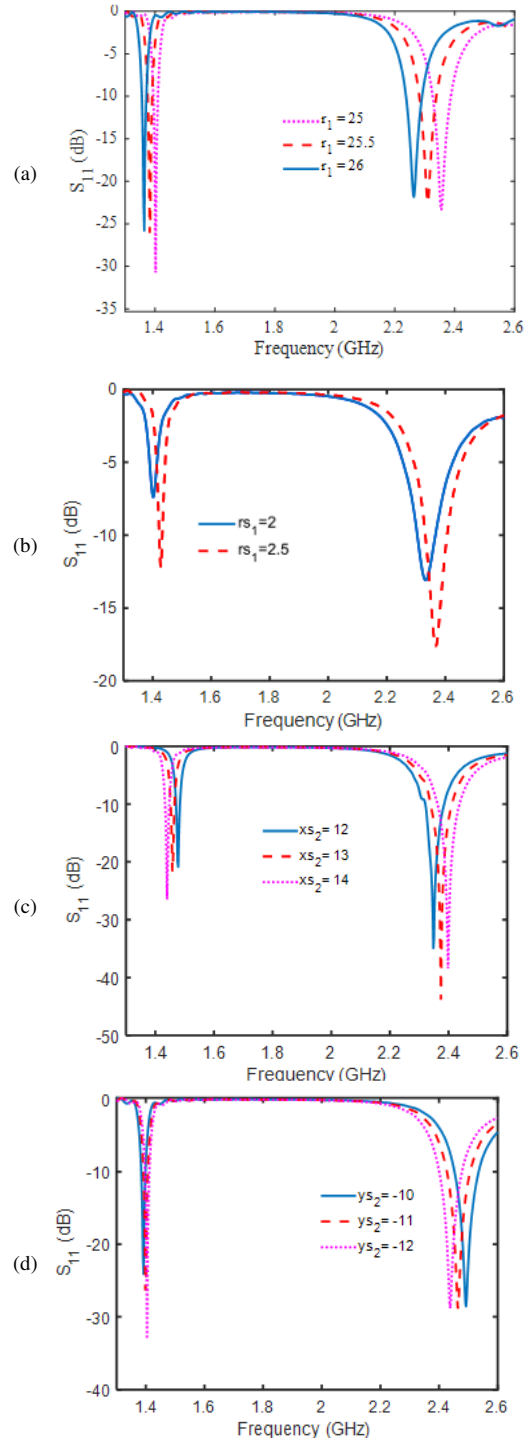


Fig. 5. Impact of various dimensions on return loss of the antenna, (a) r_1 , (b) r_{s1} , (c) x_{s2} , (d) y_{s2} . For all parameters, consider origin at the center of the antenna.

The two PTHs were also implemented along with the pads and vias and the cylindrical conductors with the required radii were inserted into the PTHs and soldered only between the top and bottom layers. The side-by-side view of the antenna prototype is displayed in Figure 6, where the two substrates were mounted in a single package using screws at the four edges, which helped to align the substrates along with reducing the air gap effect to a minimum. Subsequently, the fabricated prototype was subjected to measurement using a Vector Network Analyzer (VNA). The measured return loss of the antenna is presented in Figure 7, which also depicts the simulated response of the final prototype, as predicted by CST MWS. As shown in Figure 7, there is a notable correlation between the simulated and measured results.

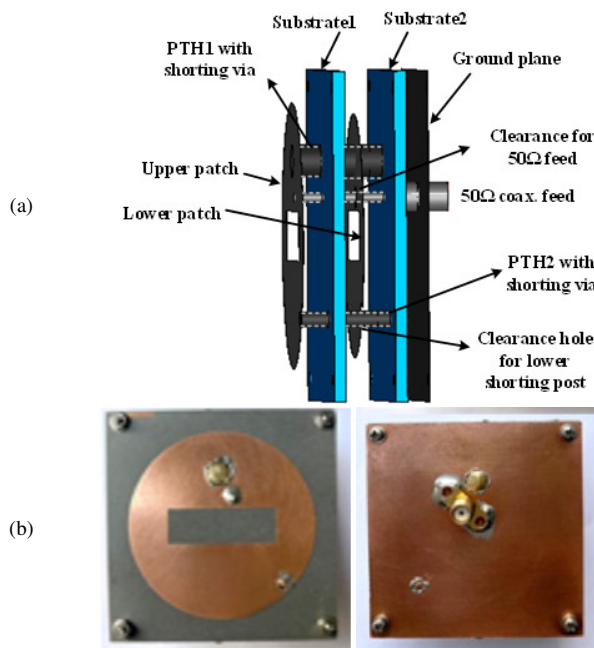


Fig. 6. (a) Juxtaposed view of the antenna package for overall measurement (b) photograph of the top view (left) and bottom view (right) of the final manufactured prototype.

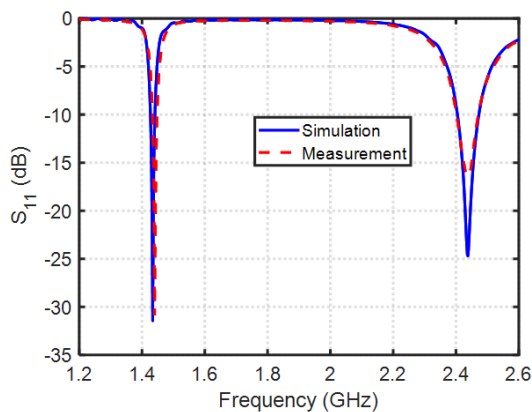


Fig. 7. Simulated and measured return loss of the antenna.

The measured radiation patterns of the antenna are also presented in Figure 8, which is compared to the radiation patterns predicted using CST MWS. It is evident from the radiation pattern in various planes that the antenna successfully generates an omnidirectional radiation pattern at 1.437 GHz L-band frequencies and a broadside radiation at 2.4 GHz ISM frequencies, thus providing the required radiation pattern diversity for both on and off-body communications.

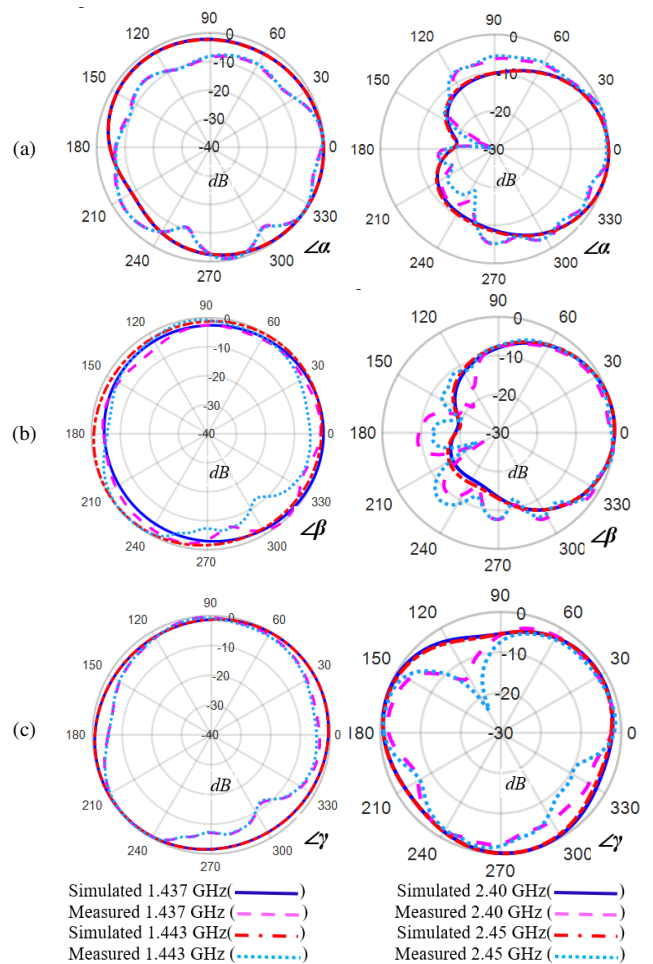


Fig. 8. Normalized radiation patterns of the antenna for the coordinate system, (a) xz plane, (b) yz plane, (c) xy plane.

IV. ON-BODY PERFORMANCE

A. Impedance Matching and Radiation Patterns

In order to examine the functionality of the antenna in the vicinity of the human body, it was essential to ascertain its performance when worn on the body. In order to conduct simulation studies, it was necessary to create a realistic human body morphology with a non-conformal surface, as would be found in reality. This is a crucial step in ensuring the reliability of the results, as using regular geometric shapes (e.g., parallelepiped) [30], may not accurately represent the human body. For this purpose, this study considered an interesting software program, POSER® [31], which is a figure posing and rendering 3D computer graphics software utilized by graphic

designers and game developers. The POSER software offers a variety of three-dimensional morphs, from which an appropriate full-body ghost phantom was selected to model a realistic adult human morphology. The phantom was imported into CST MWS, and the antenna was positioned on its chest for radio studies. However, this resulted in a computationally complex simulation problem, as the body model considered had a height of 1.8 m, similar to that of a typical adult male, in order to ensure realistic results. This led to an exceptionally large computational issue, with a complexity of $104 \times \lambda_g$ at 2.4 GHz ($\epsilon_r = 52$), necessitating the use of a mesh comprising billions of cells. To ensure a realistic computation problem size, exhaustive steps were taken to converge the mesh to a realizable simulation problem size for limited computer resources. An energy-based mesh convergence criterion was employed in CST MWS to validate the accuracy of the resulting less dense mesh, and it was ensured that the error Δ was less than 2% between passes. The resulting convergent mesh was employed in additional simulation studies, which yielded a realizable computation problem size. In order to model the human body, uniform muscle tissue properties were deployed [32]. Additionally, separate radio simulations were conducted using the specified muscle tissue parameters at 1.437 GHz ($\epsilon_r = 54.1$, $\sigma = 1.1585$ S/m) and 2.45 GHz ($\epsilon_r = 52.7$, $\sigma = 1.74$ S/m), in accordance with the values calculated by [33].

The resulting return loss of the antenna on-body model is presented in Figure 9, which compares it to that in free space and includes both simulations and measurements. The antenna demonstrates a high degree of stability in on-body performance despite its proximity to the human body. There is no discernible frequency detuning, despite the body's known tendency to detune the resonant frequency due to its high permittivity and lossy tissue. This is caused by the full ground plane at the back of the antenna, which serves to mask the radiation incidence towards the body, thereby minimizing the impact of lossy tissue.

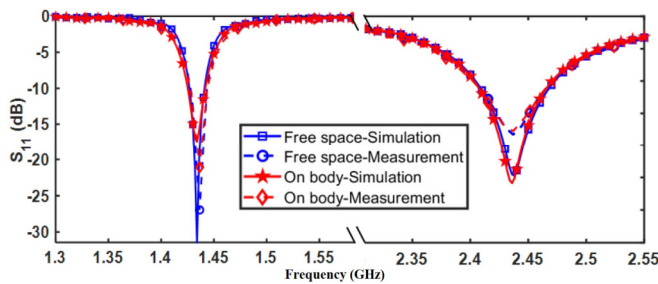


Fig. 9. Simulated and measured return loss of the antenna on human body compared to the free space counterparts.

The radiation patterns of the antenna on body model for both modes at 1.437 GHz and 2.45 GHz are presented in Figure 10, with a comparison to those in free space. It is evident that despite the minimal antenna-body spacing (and thus maximal body impact), the antenna still exhibits relatively stable radiation patterns in proximity to the human body, when compared to those observed in free space. The attenuation of the antenna radiation in the backward planes (xz and yz planes) is attributed to the high attenuation caused by human

tissue at microwave frequencies. For example, the attenuation constant $\psi = 3.9$ dB/cm at 2.45 GHz for equivalent tissue properties, demonstrates this phenomenon [34].

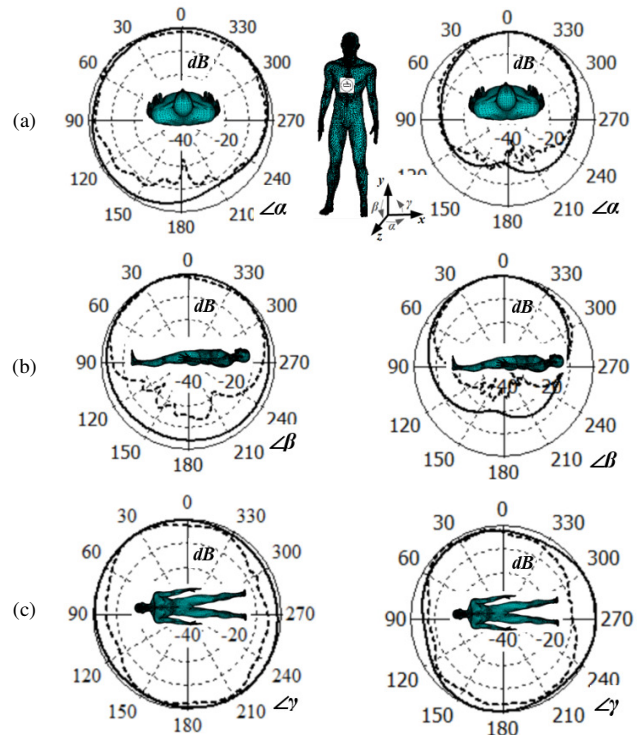


Fig. 10. Radiation patterns (normalized) of the antenna on body model (-----) compared to those in free space (——) at 1.437 GHz (left) and 2.45 GHz (right) (a) xz -plane (b) yz -plane (c) xy -plane. Coordinate system is also shown with avatar.

B. Specific Absorption Rate

In order to ascertain the compliance of the antenna for body-centric communications, it is essential to examine the quantity of electromagnetic energy absorbed by human tissue when exposed to electromagnetic radiation. The dose is given by the Specific Absorption Rate (SAR), which can be calculated using the following formula for a given tissue location [35]:

$$SAR(x, y, z) = \frac{\sigma(x, y, z)}{2\rho(x, y, z)} \left[|E_x(x, y, z)|^2 + |E_y(x, y, z)|^2 + |E_z(x, y, z)|^2 \right] \quad (1)$$

where $\sigma(x, y, z)$ and $\rho(x, y, z)$ are the conductivity (Siemens/m), and density (kg/m^3) of the tissue at the specified location. The SAR was calculated using CST MWS in accordance with the IEEE C 95.3 standard, with an averaged tissue mass of 10 g (and 1 W peak stimulated power) as specified by the Telecommunication Technology Council Agenda No. 89 and CENELEC 1995 [29]. The computed SAR across the cross-section of the body model is manifested in Figure 11.

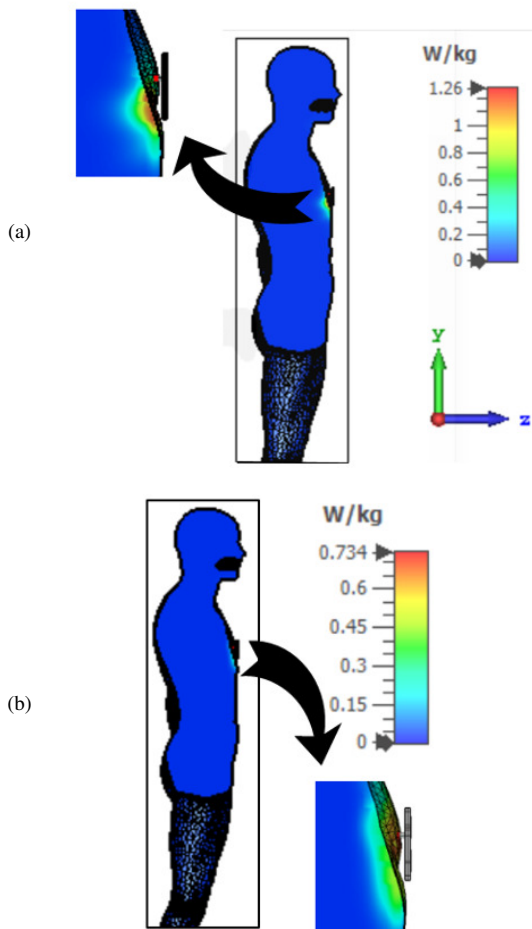


Fig. 11. 10g SAR of the antenna at (a) 1.437 GHz and (b) 2.45 GHz; cross-sectional view.

The maximum 10 g SAR of the antenna was determined to be 1.26 W/kg at 1.437 GHz and 0.734 W/kg at 2.45 GHz. The lower value of SAR at higher frequencies can be attributed to two factors: the high attenuation of the lossy tissue at higher frequencies and the broadside direction of the antenna radiation, which results in a reduced incidence on the body. Nevertheless, both evaluated values are less than the compliance standards, for example, those set forth by the EU. The SAR for a 10-gram tissue mass was found to be less than 2 W/kg [36]. The worst-case performance is presented here, even without consideration of the spacing introduced by the textile. This still lies far below the compliance limit. An increase in the antenna-body spacing will result in a notable reduction in the SAR. This evidence substantiates the assertion that the antenna is a highly promising candidate for body-centric applications while simultaneously meeting the international compliance limits for health and safety.

V. CONCLUSION

A novel dual-band antenna has been presented, which successfully generates radiation pattern diversity at 1.437 GHz L-band and ISM 2.45 GHz. As displayed in Table II, the proposed antenna exhibits the smallest electrical size in relation to the minimum operating frequency (which should correspond to the maximum wavelength and, consequently, the antenna size), while simultaneously providing both omni-directional and directional (broadside) radiation patterns at dual bands within a single planar package. Furthermore, the antenna is constructed on a Rogers Duroid substrate, which facilitates straightforward fabrication, while enabling a highly adaptable design to accommodate the desired frequency bands. The antenna performance has been validated in close proximity to the human body, with maximal body impact, and is observed to be quite stable.

TABLE II. COMPARISON OF THE PROPOSED DUAL-BAND ANTENNA WITH OTHER STUDIES

Ref.	Substrate	No. of Operating Bands	Physical size (mm ³)	Electrical size (λ_0^3) (f_{min})	Pattern type	Peak Gain dBi (Free space)	Peak Gain dBi (On Body)
[3]	Wool felt /Conductive fabric	Single	46×36×2	0.78×0.61×0.034 (5.15 GHz)	Directional	5.9	6
[6]	Flexible polyester textile	Single	34.8×39×4.5	0.66×0.74×0.08 (5.7 GHz)	Broadside	8.92	8.29
[7]	Pellon fabric	Single	102×68×3.6	1.46×0.97×0.05 (4.30 GHz)	Dipole-like /Omni-directional	6.12	6.29
[8]	Rogers Duroid 5870	Triple	35×26.6×1.6	0.37×0.28×0.017 (3.19 GHz)	Omnidirectional/ Quasi-Omnidirectional	5.50	5.05
[17]	FR4	Dual	50×50×5.2	0.40×0.40×0.04 (2.45 GHz)	Omnidirectional/ Directional	7.9	-
[18]	FR4/Felt	Single	55×55×2.6	0.42×0.42×0.02 (2.32 GHz)	Omnidirectional/ Directional	3.86	-
[23]	Taconic TLY-5/Felt	Dual	60×60×8.7	0.47×0.47×0.06 (2.39 GHz)	Directional	8.6	8.6
This work	Rogers Duroid 5870	Dual	60×60×4.4	0.28×0.28×0.02 (1.427 GHz)	Omnidirectional/ Directional	6.48	6.24

This stability is comparable to that detected in free space, in terms of both impedance matching and radiation patterns. This has been achieved through the use of a full ground plane, without the incorporation of any complex structures such as AMC or EBG. This suggests that the human body does not significantly affect the performance of the proposed antenna,

despite its lossy and dispersive nature. Furthermore, the Specific Absorption Rate (SAR) of the antenna is below the international compliance limit. This evidence substantiates the assertion that the antenna is a promising candidate for integration into wearable applications. In this study, the antenna is demonstrated as a proof of concept for applications

in the L-band and ISM band frequencies. The antenna offers a highly flexible and adaptable design, utilizing the available 14 degrees of freedom, and can be easily tuned for any desired frequency bands through the use of parametric simulations in Computer-Aided Design (CAD) tools.

ACKNOWLEDGMENT

The authors extend their appreciation to the Deputyship for Research and Innovation, Ministry of Education in Saudi Arabia for funding this research work through the project number MoE-IFG-20-06.

REFERENCES

- [1] M. A. Hanson *et al.*, "Body Area Sensor Networks: Challenges and Opportunities," *Computer*, vol. 42, no. 1, pp. 58–65, Jan. 2009, <https://doi.org/10.1109/MC.2009.5>.
- [2] T. Alves, B. Poussot, and J.-M. Laheurte, "Analytical Propagation Modeling of BAN Channels Based on the Creeping-Wave Theory," *IEEE Transactions on Antennas and Propagation*, vol. 59, no. 4, pp. 1269–1274, Apr. 2011, <https://doi.org/10.1109/TAP.2010.2096184>.
- [3] G.-P. Gao, C. Yang, B. Hu, R.-F. Zhang, and S.-F. Wang, "A Wide-Bandwidth Wearable All-Textile PIFA With Dual Resonance Modes for 5 GHz WLAN Applications," *IEEE Transactions on Antennas and Propagation*, vol. 67, no. 6, pp. 4206–4211, Jun. 2019, <https://doi.org/10.1109/TAP.2019.2905976>.
- [4] G. Gao, R. Zhang, C. Yang, H. Meng, W. Geng, and B. Hu, "Microstrip monopole antenna with a novel UC-EBG for 2.4 GHz WBAN applications," *IET Microwaves, Antennas & Propagation*, vol. 13, no. 13, pp. 2319–2323, 2019, <https://doi.org/10.1049/iet-map.2019.0271>.
- [5] S. Yan, P. J. Soh, and G. A. E. Vandenbosch, "Low-Profile Dual-Band Textile Antenna With Artificial Magnetic Conductor Plane," *IEEE Transactions on Antennas and Propagation*, vol. 62, no. 12, pp. 6487–6490, Dec. 2014, <https://doi.org/10.1109/TAP.2014.2359194>.
- [6] W. Bouamra, I. Sfar, A. Mersani, L. Osman, and J. M. Ribero, "A Low-Profile Wearable Textile Antenna Using AMC for WBAN Applications at 5.8GHz," *Engineering, Technology & Applied Science Research*, vol. 12, no. 4, pp. 9048–9055, Aug. 2022, <https://doi.org/10.48084/etasr.5011>.
- [7] A. Alemaryeen and S. Noghianian, "On-Body Low-Profile Textile Antenna With Artificial Magnetic Conductor," *IEEE Transactions on Antennas and Propagation*, vol. 67, no. 6, pp. 3649–3656, Jun. 2019, <https://doi.org/10.1109/TAP.2019.2902632>.
- [8] M. N. Shakib, M. Moghavvemi, and W. N. L. B. W. Mahadi, "Design of a Tri-Band Off-Body Antenna for WBAN Communication," *IEEE Antennas and Wireless Propagation Letters*, vol. 16, pp. 210–213, 2017, <https://doi.org/10.1109/LAWP.2016.2569819>.
- [9] S. Mallavarapu and A. Lokam, "Circuit Modeling and Analysis of Wearable Antennas on the Effect of Bending for Various Feeds," *Engineering, Technology & Applied Science Research*, vol. 12, no. 1, pp. 8180–8187, Feb. 2022, <https://doi.org/10.48084/etasr.4699>.
- [10] U. Hasni and E. Topsakal, "Wearable Antennas for On-Body Motion Detection," in *2020 IEEE USNC-CNC-URSI North American Radio Science Meeting (Joint with AP-S Symposium)*, Montreal, QC, Canada, Jul. 2020, pp. 1–2, <https://doi.org/10.23919/USNC/URSI49741.2020.9321663>.
- [11] A. S. Andrenko, I. Ida, and T. Kikuzuki, "Dual-band patch antenna with monopole-like radiation patterns for BAN communications," in *2013 7th European Conference on Antennas and Propagation (EuCAP)*, Gothenburg, Sweden, Apr. 2013, pp. 1922–1926, Accessed: Aug. 07, 2024.
- [12] T. Tuovinen, K. Y. Yazdandoost, and J. Iinatti, "Ultra Wideband loop antenna for on-body communication in Wireless Body Area Network," in *2012 6th European Conference on Antennas and Propagation (EuCAP)*, Prague, Czech Republic, Mar. 2012, pp. 1349–1352, <https://doi.org/10.1109/EuCAP.2012.6205811>.
- [13] X.-Q. Zhu, Y.-X. Guo, and W. Wu, "A Compact Dual-Band Antenna for Wireless Body-Area Network Applications," *IEEE Antennas and Wireless Propagation Letters*, vol. 15, pp. 98–101, 2016, <https://doi.org/10.1109/LAWP.2015.2431822>.
- [14] L. Zhang, J. Li, Y. Wang, S. Yan, K.-D. Xu, and H. Luyen, "A Compact Dual-Band Wearable Button Antenna Design for WBAN Applications," *IEEE Transactions on Antennas and Propagation*, vol. 71, no. 10, pp. 8284–8289, Oct. 2023, <https://doi.org/10.1109/TAP.2023.3292476>.
- [15] Y. Hong, J. Tak, and J. Choi, "Dual-band dual-mode patch antenna for on–on–off WBAN applications," *Electronics Letters*, vol. 50, no. 25, pp. 1895–1896, 2014, <https://doi.org/10.1049/el.2014.2551>.
- [16] R. B. V. B. Simorangkir, Y. Yang, K. P. Esselle, L. Matekovits, and S. M. Abbas, "A simple dual-band dual-mode antenna for off-/on-body centric communications," in *2016 10th European Conference on Antennas and Propagation (EuCAP)*, Davos, Switzerland, Apr. 2016, pp. 1–3, <https://doi.org/10.1109/EuCAP.2016.7481221>.
- [17] C. Zhao and W. Geyi, "Design of a dual band dual mode antenna for on/off body communications," *Microwave and Optical Technology Letters*, vol. 62, no. 1, pp. 514–520, 2020, <https://doi.org/10.1002/mop.32085>.
- [18] G.-P. Gao, B.-K. Zhang, J.-H. Dong, Z.-H. Dou, Z.-Q. Yu, and B. Hu, "A Compact Dual-Mode Pattern-Reconfigurable Wearable Antenna for the 2.4-GHz WBAN Application," *IEEE Transactions on Antennas and Propagation*, vol. 71, no. 2, pp. 1901–1906, Feb. 2023, <https://doi.org/10.1109/TAP.2022.3225529>.
- [19] S. Ahmad, A. Ghaffar, N. Hussain, and N. Kim, "Compact Dual-Band Antenna with Paired L-Shape Slots for On- and Off-Body Wireless Communication," *Sensors*, vol. 21, no. 23, Jan. 2021, Art. no. 7953, <https://doi.org/10.3390/s21237953>.
- [20] S. Raman *et al.*, "Microstrip fed ground modified compact antenna with reconfigurable radiation pattern for BANs," in *2012 Loughborough Antennas & Propagation Conference (LAPC)*, Loughborough, UK, Nov. 2012, pp. 1–4, <https://doi.org/10.1109/LAPC.2012.6403038>.
- [21] J. Tak, S. Woo, J. Kwon, and J. Choi, "Dual-Band Dual-Mode Patch Antenna for On-/Off-Body WBAN Communications," *IEEE Antennas and Wireless Propagation Letters*, vol. 15, pp. 348–351, 2016, <https://doi.org/10.1109/LAWP.2015.2444881>.
- [22] H. Liu, L. Meng, X. Huo, S. Liu, and J. Xiao, "A Novel Dual-Band Dual-Pattern Radiation Patch Antenna Based on Mode Analysis Theory Under TM01 and TM02 Mode," in *2020 IEEE MTT-S International Conference on Numerical Electromagnetic and Multiphysics Modeling and Optimization (NEMO)*, Hangzhou, China, Dec. 2020, pp. 1–4, <https://doi.org/10.1109/NEMO49486.2020.9343624>.
- [23] T. T. Le and T.-Y. Yun, "Wearable Dual-Band High-Gain Low-SAR Antenna for Off-Body Communication," *IEEE Antennas and Wireless Propagation Letters*, vol. 20, no. 7, pp. 1175–1179, Jul. 2021, <https://doi.org/10.1109/LAWP.2021.3074641>.
- [24] U. Musa *et al.*, "Design and Analysis of a Compact Dual-Band Wearable Antenna for WBAN Applications," *IEEE Access*, vol. 11, pp. 30996–31009, 2023, <https://doi.org/10.1109/ACCESS.2023.3262298>.
- [25] G.-P. Gao, H.-J. Meng, W.-F. Geng, Z.-H. Dou, B.-K. Zhang, and B. Hu, "A Wideband Metasurface Antenna With Dual-Band Dual-Mode for Body-Centric Communications," *IEEE Antennas and Wireless Propagation Letters*, vol. 21, no. 1, pp. 149–153, Jan. 2022, <https://doi.org/10.1109/LAWP.2021.3121585>.
- [26] B. Wang, S. Yan, and Y. He, "A CRLH-TL Inspired Dual-Band Antenna With Polarization Diversity for Wrist-Worn Wireless Body Area Network Devices," *IEEE Transactions on Antennas and Propagation*, vol. 71, no. 6, pp. 4812–4822, Jun. 2023, <https://doi.org/10.1109/TAP.2023.3263944>.
- [27] P. B. Samal, S. J. Chen, and C. Fumeaux, "Flexible Hybrid-Substrate Dual-Band Dual-Mode Wearable Antenna," *IEEE Transactions on Antennas and Propagation*, vol. 72, no. 2, pp. 1286–1296, Feb. 2024, <https://doi.org/10.1109/TAP.2023.3332432>.
- [28] R. Garg, P. Bharti, I. Bahl, and A. Ittipiboon, *Microstrip Antenna Design Handbook*. Norwood, MA, USA: Artech House, 2001.
- [29] "CST Studio Suite," *Dassault Systèmes*, Jul. 25, 2023. <https://www.3ds.com/products/simulia/cst-studio-suite>.

-
- [30] M. Kouchi, "Human body dimensions data for ergonomic design," Report of National Institute of Bioscience and Human-Technology 2, 1994.
- [31] "Poser - 3D Rendering & Animation Software." <https://www.posersoftware.com/>.
- [32] J. Naganawa, K. Wangchuk, M. Kim, T. Aoyagi, and J. Takada, "Simulation-Based Scenario-Specific Channel Modeling for WBAN Cooperative Transmission Schemes," *IEEE Journal of Biomedical and Health Informatics*, vol. 19, no. 2, pp. 559–570, Mar. 2015, <https://doi.org/10.1109/JBHI.2014.2326424>.
- [33] D. Andreuccetti and R. Fossi, "Dielectric Properties of Human Tissues: Definitions, Parametric Model, Computing Codes," Istituto Di Ricerca Sulle Onde Elettromagnetiche, Firenze, Italy, IROE Technical Report N.TR/ICEMM/13.00, Sep. 2000. [Online]. Available: <http://niremf.ifac.cnr.it/tissprop/>.
- [34] I. Yamaura, "Measurements of 1.8 - 2.7-Ghz Microwave Attenuation in the Human Torso," *IEEE Transactions on Microwave Theory and Techniques*, vol. 25, no. 8, pp. 707–710, Aug. 1977, <https://doi.org/10.1109/TMTT.1977.1129191>.
- [35] F. Kaburcuk and A. Elsherbeni, "Temperature rise and SAR distribution at wide range of frequencies in a human head due to an antenna radiation," *Applied Computational Electromagnetics Society Journal*, vol. 33, pp. 367–372, Nov. 2018.
- [36] "Mobiltelefoner och Strålning," The Swedish Radiation Safety Authority, Technical Report, 2003.